Angular and polarization properties of the Lyman-α_1 line $2p_{3/2} \rightarrow 1s_{1/2}$ following electron-impact excitation of hydrogenlike ions

Z. W. Wu [1,2,3,*] Z. M. He,[1] Z. Q. Tian,[1] C. Z. Dong,[1] and S. Fritzsche [2,3,4]

[1]*Key Laboratory of Atomic and Molecular Physics & Functional Materials of Gansu Province, College of Physics and Electronic Engineering, Northwest Normal University, Lanzhou 730070, People's Republic of China*

[2]*Helmholtz-Institut Jena, Fröbelstieg 3, D-07743 Jena, Germany*

[3]*GSI Helmholtzzentrum für Schwerionenforschung GmbH, Planckstrasse 1, D-64291 Darmstadt, Germany*

[4]*Theoretisch-Physikalisches Institut, Friedrich-Schiller-Universität Jena, Max-Wien-Platz 1, D-07743 Jena, Germany*

(Received 28 March 2022; accepted 2 June 2022; published 21 June 2022)

Electron-impact excitation from the ground state to the excited energy level $2p_{3/2}$ of hydrogenlike ions and subsequent Lyman-α_1 ($2p_{3/2} \rightarrow 1s_{1/2}$) radiative decay are investigated using the relativistic distorted-wave method. Special attention is paid to the linear polarization and angular distribution of the Lyman-α_1 line and also to the effects of the Breit interaction. To this aim, detailed calculations are performed for hydrogenlike Ti^{21+}, Mo^{41+}, Ba^{55+}, and Au^{78+} ions. It is found that the presently obtained (partial cross sections and) linear polarization agree excellently with other theoretical and experimental results available for low-Z Ti^{21+} ions within the experimental uncertainties. Moreover, the Lyman-α_1 line is found to be less linearly polarized and less anisotropic due to the contribution of the Breit interaction. Such effects of the Breit interaction behave more prominently for higher-Z ions and higher impact electron energies, respectively. For instance, the Breit interaction qualitatively changes the polarization behavior and angular emission pattern of the Lyman-α_1 line from high-Z Au^{78+} ions at the impact energy of about 4.2 times the corresponding excitation threshold.

DOI: 10.1103/PhysRevA.105.062813

I. INTRODUCTION

Angular distribution and linear polarization of characteristic (x-ray) lines have been studied for many decades, both theoretically and experimentally. Due to their good sensitivities, they have been employed as an effective tool to explore various physical effects and interactions, such as, the Breit interaction [1–10], hyperfine interaction [11–14], spin-orbit interaction [15], relativistic effects [16,17], and spin-polarization effects [18–20], and to reveal also multipole mixing of radiation fields [21,22], level splitting and sequence of (hyper)fine-structure resonances [23–25], and formation mechanism of characteristic spectral lines [26].

Electron-impact excitation (EIE) of atoms and ions is one of the fundamental processes in astrophysical and laboratory plasmas, which is thus an important mechanism of inducing line emissions. During past decades, the angular and polarization properties of characteristic lines following EIE of atoms and ions have been attracting a lot of attention [27–38]. For example, Reed and Chen studied linear polarization of the Lyman-α_1 line ($2p_{3/2} \rightarrow 1s_{1/2}$) following EIE of hydrogenlike Ti^{21+}, Mo^{41+}, Ba^{55+}, and Au^{78+} ions with the use of the relativistic distorted-wave (RDW) method [39]. It was found that the linear polarization is independent of atomic number Z in the nonrelativistic limit, whereas it becomes markedly Z dependent when the relativistic effects are taken into consideration. Afterwards, Nakamura *et al.* estimated the linear polarization for Ti^{21+} ions by means of the measured intensity ratio of the Lyman-$\alpha_{1,2}$ lines at the Tokyo electron-beam ion trap (EBIT) and the calculated total emission cross section ratio [40]. They found that their experimental results are systematically smaller than the theoretical ones from Ref. [39] at all impact electron energies considered, although it has been pointed out that the values of the linear polarization in Table II of Ref. [39] are inconsistent with those from Fig. 3 therein. Similar discrepancies were found by Robbins *et al.* for hydrogenlike Ar^{17+} and Fe^{25+} ions [41] and were also highlighted by Beiersdorfer in a review of spectroscopy with trapped highly charged ions [42]. Soon after, Bostock *et al.* studied the linear polarization for hydrogenlike Ar^{17+}, Ti^{21+}, and Fe^{25+} ions using the relativistic convergent close-coupling (RCCC) method and found that account of the Breit interaction is essential to resolve the existing discrepancies between experiment and theory [43,44]. In the relativistic non-Breit case, nevertheless, the RCCC results for the linear polarization of the Lyman-α_1 line were found to be much different from those obtained using the RDW method, especially at low impact electron energies [39,44], however, which was never addressed thereafter. In addition, as one of the main properties, the angular emission behavior of the Lyman-α_1 line was hardly explored, in sharp contrast to the intensive studies on its polarization behavior.

In the present work, we study the EIE of hydrogenlike Ti^{21+}, Mo^{41+}, Ba^{55+}, and Au^{78+} ions from their ground-state level $1s_{1/2}$ to the excited energy level $2p_{3/2}$ as well as the subsequent Lyman-α_1 ($2p_{3/2} \rightarrow 1s_{1/2}$) decay with the use of

*zhongwen.wu@nwnu.edu.cn

the RDW method. Special attention is paid to the angular and polarization behaviors of the Lyman-α_1 line and particularly to the effect of the Breit interaction on both. For this purpose, we first calculate partial EIE cross sections from the ground state to individual magnetic substates of the excited energy level. These partial EIE cross sections are then employed to calculate alignment parameters of the excited level $2p_{3/2}$ and, further, obtain linear polarization and angular distribution of the Lyman-α_1 line. It is found that the present partial cross sections and linear polarization agree excellently with the RCCC results [44] available for Ti^{21+} ions, although discrepancies with the RDW results of Reed and Chen [39] are found for the case without the Breit interaction included. In the real case with the Breit interaction considered, the present linear polarization coincides well with the experimental results of Ti^{21+} ions [40] within the experimental uncertainties. In addition, the Lyman-α_1 line is found to be less linearly polarized and less anisotropic due to the contribution of the Breit interaction, which behaves more prominently for higher-Z ions and higher impact electron energies. For example, the polarization and angular emission pattern of the Lyman-α_1 line from high-Z Au^{78+} ions are qualitatively altered due to the Breit interaction at the impact energy of about 4.2 times the excitation threshold.

The rest of this paper is structured as follows. In the next section, the theoretical method will be presented for partial EIE cross sections as well as for linear polarization and angular distribution of the Lyman-α_1 line. Then, in Sec. III we shall elaborate the presently obtained linear polarization and angular distribution and show how they are affected by the Breit interaction. Finally, the present work will be summarized briefly in Sec. IV. Atomic units are used throughout the paper unless stated otherwise.

II. THEORETICAL METHOD

In the present work, the partial EIE cross sections involved are calculated with the use of a RDW computer program REIE06 [45]. Since the RDW method has been introduced in great detail in many literatures (refer to, for instance, Refs. [46,47]), here we just recall its central content for brevity. In the RDW method, if the direction of incoming impact electrons is chosen as the quantization axis z, the projection of orbital angular momentum l_i (l_i') of the impact electron onto the z axis is zero, i.e., $m_{l_i}=m_{l_i'}=0$. Under this condition, the partial cross sections for a particular EIE process from a well-defined initial state $|\beta_i J_i M_i\rangle$ to a well-defined final state $|\beta_f J_f M_f\rangle$ of target ions can be expressed as [48]

$$\sigma_{|i\rangle\to|f\rangle}(\varepsilon_i)=\frac{2\pi a_0^2}{k_i^2}\sum_{l_i j_i l_i' j_i' m_{s_i}}\sum_{l_f j_f m_f}\sum_{JJ'M} i^{l_i-l_i'}[l_i,l_i']^{1/2}\exp\left[i(\delta_{\kappa_i}-\delta_{\kappa_i'})\right]\langle l_i m_{l_i},1/2\,m_{s_i}|j_i m_i\rangle\langle l_i' m_{l_i'},1/2\,m_{s_i}|j_i' m_i\rangle$$
$$\times\langle J_i M_i, j_i m_i|JM\rangle\langle J_i M_i, j_i' m_i|J'M\rangle\langle J_f M_f, j_f m_f|JM\rangle\langle J_f M_f, j_f m_f|J'M\rangle R(\gamma_i,\gamma_f)R^*(\gamma_i',\gamma_f'). \quad (1)$$

In this equation, the subscripts i and f indicate the initial and final states of systems or quantities involved, respectively. l_i, $1/2$, and j_i are orbital, spin, and total angular momenta of the impact electron, respectively, while m_{l_i}, m_{s_i}, and m_i are their projections onto the quantization z axis. β_i denotes all other quantum numbers for a unique specification of the initial state $|\beta_i J_i M_i\rangle$ in addition to its total angular momentum J_i and z-projection M_i. $J(J')$ and M are total angular momentum of the impact system (i.e., the target ion plus the impact electron) and its projection onto the z axis, respectively. $\gamma_i\equiv(\varepsilon_i l_i j_i \beta_i J_i JM)$. κ_i is the relativistic quantum number of the impact electron and is uniquely determined by l_i and j_i. Other quantum numbers with the subscript f have meanings similar to those stated above but for the related final states. δ_{κ_i} is the phase shift of the impact electron. k_i denotes the relativistic wave number of the impact electron, which is simply related to its kinetic energy (i.e., impact energy) ε_i (in rydbergs) by $k_i^2=\varepsilon_i(1+\alpha^2\varepsilon_i/4)$ with fine-structure constant α. a_0 is the Bohr radius. Furthermore, the standard notation of the Clebsch-Gordan coefficients and the shorthand notation $[a,b,...]\equiv(2a+1)(2b+1)...$ have been used. In addition, $R(\gamma_i,\gamma_f)$ denotes the EIE amplitudes, which can be formally expressed as

$$R(\gamma_i,\gamma_f)=\langle\psi_{\gamma_f}|\sum_{p,q;p<q}^{N+1}\left(\frac{1}{r_{pq}}+V_{\rm Breit}\right)|\psi_{\gamma_i}\rangle. \quad (2)$$

Here, ψ_{γ_i} and ψ_{γ_f} denote antisymmetric $(N+1)$-electron wave functions for the initial and final states of the impact system, respectively. Besides the Coulomb potential $1/r_{pq}$, we here incorporate also the Breit interaction, as shown below, into the EIE amplitudes because of its particular importance [49],

$$V_{\rm Breit}=-\frac{\boldsymbol{\alpha}_p\cdot\boldsymbol{\alpha}_q}{r_{pq}}\cos(\omega_{pq}r_{pq})$$
$$+(\boldsymbol{\alpha}_p\cdot\boldsymbol{\nabla}_p)(\boldsymbol{\alpha}_q\cdot\boldsymbol{\nabla}_q)\frac{\cos(\omega_{pq}r_{pq})-1}{\omega_{pq}^2 r_{pq}}, \quad (3)$$

where $\boldsymbol{\alpha}_p$ and $\boldsymbol{\alpha}_q$ are the Dirac matrix vectors of electrons p and q, respectively. ω_{pq} is the angular frequency of virtual photons exchanged between electrons. ∇_p represents the vector gradient operator associated with electron p.

Having the substate-resolved partial EIE cross sections (1) ready, the relative population of individual magnetic substates $|\beta_f J_f M_f\rangle$ of the excited energy level $\beta_f J_f$ will be known, which fully determines linear polarization and angular distribution of subsequently radiated photons. In the density matrix theory [50,51], such a relative population is usually characterized by a set of alignment parameters. For the presently considered $2p_{3/2}$ level of hydrogenlike ions, only one (second-rank) alignment parameter $\mathcal{A}_{20}$ is required, which can be

expressed as [39,50]

$$\mathcal{A}_{20}(2p_{3/2}) = \frac{\sigma_{|\pm 3/2\rangle} - \sigma_{|\pm 1/2\rangle}}{\sigma_{|\pm 3/2\rangle} + \sigma_{|\pm 1/2\rangle}}. \quad (4)$$

In this expression, $\sigma_{|\pm 1/2\rangle}$ and $\sigma_{|\pm 3/2\rangle}$ denote partial EIE cross sections corresponding to the excitations from the ground-state level $1s_{1/2}$ to individual magnetic substates $|M_f = \pm 1/2\rangle$ and $|M_f = \pm 3/2\rangle$ of the excited $2p_{3/2}$ level of hydrogenlike ions, respectively, which can be obtained from the (substate-resolved) partial EIE cross sections as given by Eq. (1).

Once the alignment parameter $\mathcal{A}_{20}(2p_{3/2})$ of the $2p_{3/2}$ level is known, it completely determines the linear polarization and angular distribution of the subsequently radiated Lyman-α_1 line within the electric-dipole approximation. For instance, the linear polarization of the Lyman-α_1 line radiated perpendicularly to the incoming direction of impact electrons is given by [39]

$$P = -\frac{3\,\mathcal{A}_{20}(2p_{3/2})}{4 - \mathcal{A}_{20}(2p_{3/2})}. \quad (5)$$

In experiment, the linear polarization can be determined by recording the yields of the Lyman-α_1 photons which are linearly polarized parallel and perpendicular to the incoming electron beam, respectively.

In addition, the angular distribution of the Lyman-α_1 photons is most generally parametrized as follows if they are observed at given azimuthal angles [50],

$$\mathrm{W}(\theta) \propto 1 + \beta_2(2p_{3/2} \to 1s_{1/2})\, P_2(\cos\theta). \quad (6)$$

Here, $P_2(\cos\theta)$ is the second-order Legendre polynomial as a function of the polar angle θ of the Lyman-α_1 photons, which is determined by the directions of the incoming impact electrons and the radiated Lyman-α_1 photons. Moreover, β_2 denotes the so-called anisotropy parameter and is given by [21]

$$\beta_2(2p_{3/2} \to 1s_{1/2}) = \tfrac{1}{2}\mathcal{A}_{20}(2p_{3/2}). \quad (7)$$

So long as the anisotropy parameter $\beta_2(2p_{3/2} \to 1s_{1/2})$ is known, as seen obviously from Eq. (6), the corresponding Lyman-α_1 angular distribution will be fully determined. In experiment, the angular distribution can be obtained by recording the yields of the Lyman-α_1 photons radiated at different polar angles for fixed azimuthal angles.

As seen from Eqs. (1)–(7), further analysis of polarization and angular properties of the Lyman-α_1 line needs to be traced back to the calculations of the partial EIE cross sections of hydrogenlike ions. However, as this quantity appears frequently in the studies of EIE and radiative decay of atoms and ions and, actually, can be readily calculated with different computer programs [45,52–54], here we merely make a concise description on their calculation instead of theoretical details. The required energy levels and wave functions are generated using the GRASP2K package [52], in which the quantum-electrodynamical effect is taken into account. These energy levels and wave functions are used further to calculate the required EIE cross sections with the RDW program REIE06 [45], as stated above, in which maximal partial waves of impact electrons are chosen to be $\kappa = \pm 50$ in order to guarantee convergence. It should be noted that except for the calculations of energy levels and wave functions all other calculations are performed twice, i.e., without (NB) and with (B) the Breit interaction included, respectively.

TABLE I. Presently calculated excitation energies (eV) from the ground state $1s_{1/2}$ to the $2p_{3/2}$ level of hydrogenlike Ti^{21+}, Mo^{41+}, Ba^{55+}, and Au^{78+} ions, compared with other theoretical results from the NIST [55,56].

Ions	Ti^{21+}	Mo^{41+}	Ba^{55+}	Au^{78+}
Pres.	4979.304	18558.206	33838.961	71764.278
Ref. [55]	4976.931	18536.826	33782.080	71570.628
Ref. [56]	4976.892	18536.713		

III. RESULTS AND DISCUSSION

In Table I, we list the presently calculated excitation energies from the ground state to the $2p_{3/2}$ level of hydrogenlike Ti^{21+}, Mo^{41+}, Ba^{55+}, and Au^{78+} ions together with other theoretical results from the National Institute of Standards and Technology (NIST) [55,56] for comparison. As seen from Table I, the present excitation energies coincide very well with these available results. To be specific, the relative discrepancy is found to be within 0.05% for Ti^{21+} ions, while even for high-Z Au^{78+} ions a small discrepancy of about 0.27% is achieved.

To further account for the reliability of the present calculations, in Fig. 1 we compare the present partial EIE cross sections of Ti^{21+} ions with other available results calculated by Reed and Chen using the RDW method [39] and Bostock *et al.* using the RCCC method [43,44]. Results are plotted as a function of impact electron energy in units of the $2p_{3/2}$ excitation threshold 4979.304 eV of Ti^{21+} ions for both the NB and B cases. It is noted that the lowest impact energy employed in the present work is 1.1 times the excitation

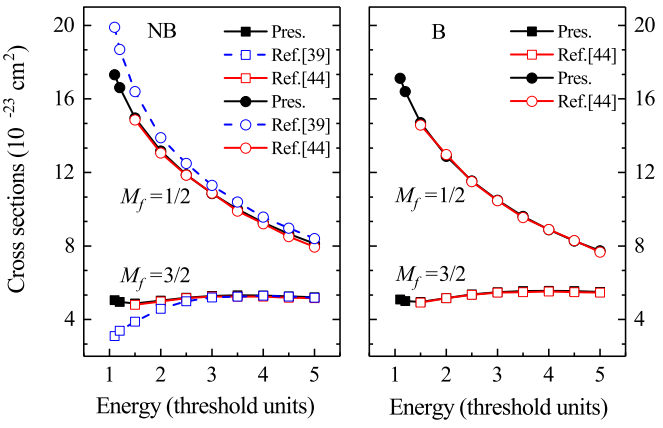

FIG. 1. Comparison of the present partial EIE cross sections (black solid lines) with other theoretical results from Reed and Chen [39] (blue dashed lines) and from Bostock *et al.* [43,44] (red solid lines) for the excitations from the ground-state level $1s_{1/2}$ to the individual magnetic substates $|M_f = \pm 1/2\rangle$ (circles) and $|M_f = \pm 3/2\rangle$ (squares) of the $2p_{3/2}$ level of Ti^{21+} ions. Results are plotted here as a function of impact electron energy in units of the excitation threshold of Ti^{21+} ions (i.e., 4979.304 eV) for both the NB (left) and B (right) cases.

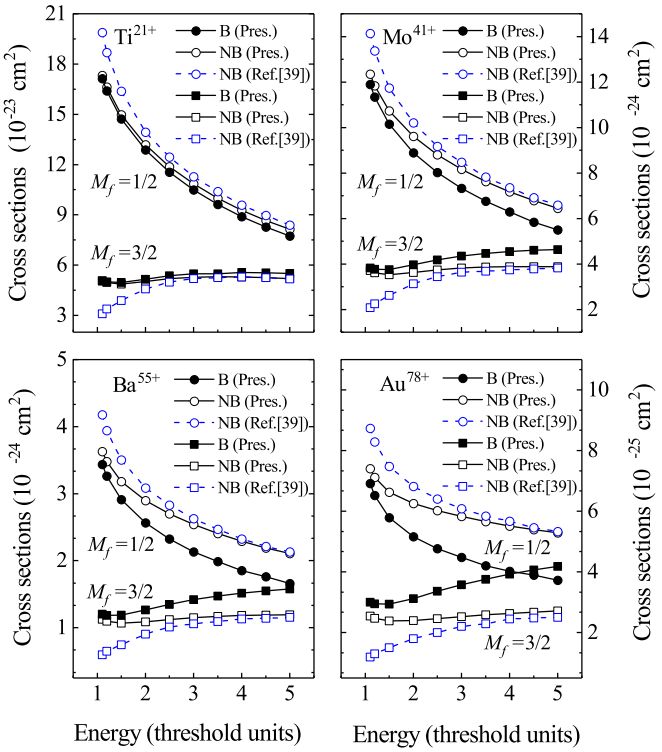

FIG. 2. Partial EIE cross sections for the excitations from the ground-state level to the magnetic substates $|M_f = \pm 1/2\rangle$ (circles) and $|M_f = \pm 3/2\rangle$ (squares) of the $2p_{3/2}$ level of Ti^{21+} (top left), Mo^{41+} (top right), Ba^{55+} (bottom left), and Au^{78+} (bottom right) ions, as a function of impact electron energy in units of their respective excitation thresholds. The present results are plotted here for both the NB (black solid lines with open symbols) and B (black solid lines with solid symbols) cases along with the NB results from Reed and Chen [39] (blue dashed lines with open symbols) for comparison.

threshold instead of itself. Moreover, it should be also noted that the partial cross sections corresponding to the substate $|M_f = -1/2\rangle$ of the $2p_{3/2}$ level are fully identical to the ones corresponding to the substate $|M_f = +1/2\rangle$ because of spatial symmetry of the excitation process of hydrogenlike ions, which is true also for both the substates $|M_f = \pm 3/2\rangle$. As can be seen obviously from Fig. 1, the present partial cross sections agree excellently with those from Bostock *et al.* [43,44] for all the impact energies considered and also for both the NB and B cases, although different theoretical methods were used by Bostock *et al.* and us, respectively. For the available NB case, in contrast, although the results of Reed and Chen [39] agree well with those from us at high impact energies, the discrepancy between them exists at low energies, which becomes more pronounced with decreasing impact energies and reaches its maximum near the excitation threshold. As the calculation details were not given in Ref. [39], we performed a series of additional calculations using different numbers of partial waves of impact electrons in order to explore the reason for such a discrepancy. Unfortunately, the number of partial waves used seems not to be the reason and, thus, this is still an open question for further studies.

Based on the comparisons above, we extended our calculations of the partial EIE cross sections to medium- and high-Z ions. For example, Fig. 2 displays the presently calculated partial cross sections associated with the individual substates $|M_f = \pm 1/2\rangle$ and $|M_f = \pm 3/2\rangle$ of Ti^{21+}, Mo^{41+}, Ba^{55+}, and Au^{78+} ions, as a function of impact energy in units of their respective excitation thresholds as listed in Table I. The present results are plotted here for both the NB and B cases together with the NB results available from Reed and Chen [39] for comparison. As seen from Fig. 2, similar to the case of Ti^{21+} ions, for the other three ions the present partial EIE cross sections without inclusion of the Breit interaction agree well with the results from Reed and Chen [39] at high impact energies, but the discrepancies between them exist at medium and low energies and become more pronounced at lower impact energies. In addition, it is found that the Breit interaction makes the substates $|M_f = \pm 1/2\rangle$ less populated, whereas it contributes to increasing the partial EIE cross sections of the $|M_f = \pm 3/2\rangle$ ones. Such effects of the Breit interaction become more and more prominent with increasing impact electron energy and atomic number of hydrogenlike ions, respectively. As can be deduced from Eq. (4), such a (completely opposite) effect of the Breit interaction on the partial cross sections of the substates $|M_f = \pm 1/2\rangle$ and $|M_f = \pm 3/2\rangle$ will alter the relative population of the $2p_{3/2}$ level, which is expected to ultimately affect the linear polarization and angular distribution of the Lyman-α_1 line radiated in the subsequent decay.

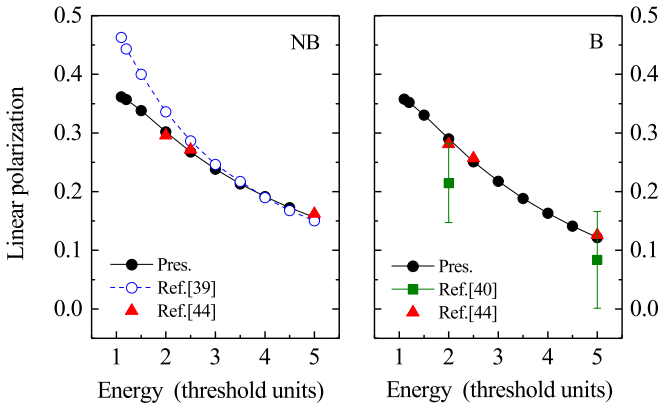

FIG. 3. Comparison of the present linear polarization (black solid circles) of the Lyman-α_1 line of Ti^{21+} ions with other theoretical results from Reed and Chen [39] (blue open circles) and Bostock *et al.* [44] (red solid triangles) and also with the experimental results from Nakamura *et al.* [40] (green solid squares). Results are given as a function of impact energy in units of the excitation threshold 4979.304 eV for both the NB (left) and B (right) cases.

In Fig. 3, we compare the presently obtained linear polarization of the Lyman-α_1 line of Ti^{21+} ions with other theoretical [39,44] and experimental [40] results for both the NB and B cases. As seen from this figure, the present RDW results agree excellently with the RCCC ones from Bostock *et al.* [44] for both the cases. In addition, in the NB case, the present linear polarization for medium and high impact energies is well consistent with the RDW results from Reed and Chen [39], whereas for low impact energies both of them differs obviously from each other, which becomes more prominent at lower energies. Moreover, in the real case with

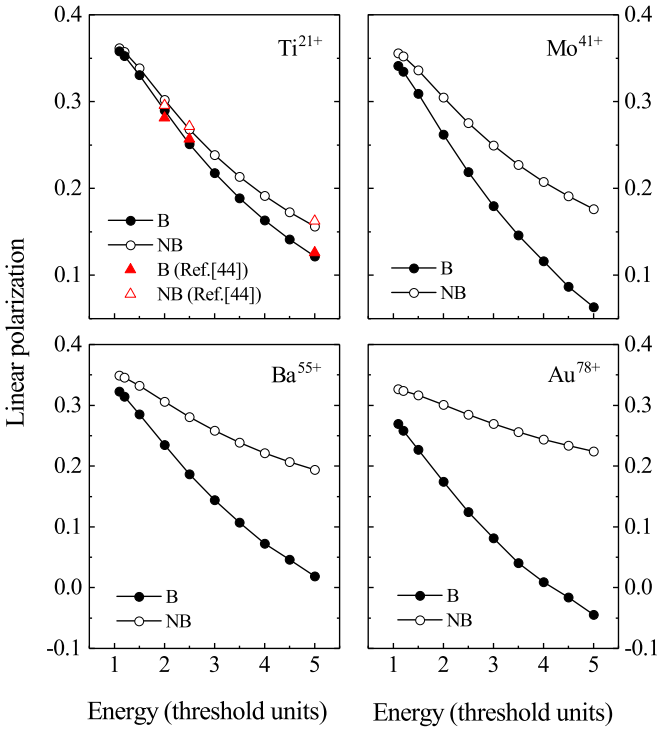

FIG. 4. Linear polarization of the Lyman-α_1 line of Ti^{21+} (top left), Mo^{41+} (top right), Ba^{55+} (bottom left), and Au^{78+} (bottom right) ions as a function of impact energy in units of their respective excitation thresholds. The present results are given for both the NB (black solid lines with open circles) and B (black solid lines with solid circles) cases for comparison, along with the RCCC results of Ti^{21+} ions from Bostock *et al*. [44] (red triangles).

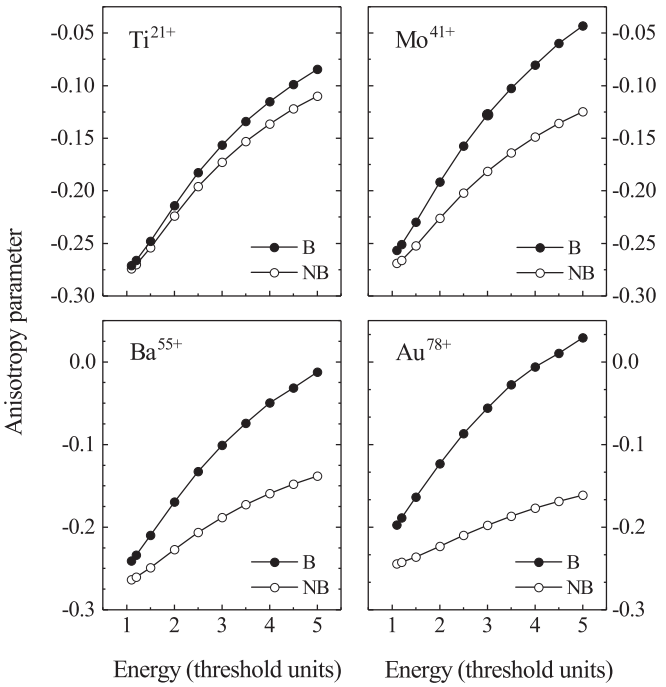

FIG. 5. Anisotropy parameters β_2 of the Lyman-α_1 line radiated from Ti^{21+} (top left), Mo^{41+} (top right), Ba^{55+} (bottom left), and Au^{78+} (bottom right) ions as a function of impact energy in units of their respective excitation thresholds. Results are shown for both the NB (open circles) and B (solid circles) cases for comparison.

the Breit interaction included, even though the present linear polarization is larger than the experimental results from Nakamura *et al.* [40], they still coincide with each other within the experimental uncertainties, especially at high impact energy.

Besides low-Z Ti^{21+} ions, we also calculated the linear polarization of the Lyman-α_1 line radiated from medium- and high-Z Mo^{41+}, Ba^{55+}, and Au^{78+} ions, which is plotted in Fig. 4 as a function of impact energy for both the NB and B cases for comparison. As can be seen obviously from Fig. 4, the Breit interaction makes the Lyman-α_1 line of these ions less linearly polarized for all the impact energies considered, and such an effect of the Breit interaction becomes more prominent with increasing impact energy and atomic number Z, respectively. For instance, for medium-Z Ba^{55+} ions the absolute contribution of the Breit interaction to the linear polarization varies quickly from 0.027 to 0.175 with the increase of the impact energy from 1.1 to 5.0 times the excitation threshold, and at the impact energy of 5.0 times their respective excitation thresholds such an absolute contribution increases from 0.035 for Ti^{21+} ions to 0.268 for Au^{78+} ions. Moreover, taking Au^{78+} ions, for example, the polarization behavior of the Lyman-α_1 line is qualitatively altered at the impact energy of about 4.2 times the excitation threshold due to the contribution of the Breit interaction.

In contrast to the extensive studies on the linear polarization of the Lyman-α_1 line following EIE of hydrogenlike ions [39–44], its angular emission behavior has hardly been addressed. On this account, apart from the linear polarization as discussed above, here we also explore the angular distribution of the Lyman-α_1 line following EIE of hydrogenlike Ti^{21+}, Mo^{41+}, Ba^{55+}, and Au^{78+} ions. In Fig. 5, we plot the presently calculated anisotropy parameters of the Lyman-α_1 line radiated from these ions as a function of impact energy. Again, results are shown for both the NB and B cases for comparison. It is found that the Lyman-α_1 line of all the ions behaves less anisotropically with increasing impact energy in both the two cases, although with different specific behaviors. Moreover, it is also found that for all of these ions the Breit interaction contributes to making the Lyman-α_1 line less anisotropic at all the impact energies considered. Similar to the case for the linear polarization of the Lyman-α_1 line, such an effect of the Breit interaction behaves more prominently at higher impact energies and for higher-Z hydrogenlike ions, respectively. Taking medium-Z Ba^{55+} ions, for example, the anisotropy parameter of the Lyman-α_1 line for the NB case changes smoothly from -0.263 to -0.138 within the impact energy range used, whereas it changes quickly from -0.241 to -0.012 when the Breit interaction is taken into consideration. At the impact energy of 5.0 times the excitation thresholds, for instance, the absolute contribution of the Breit interaction to the anisotropy parameter changes significantly from 0.025 for low-Z Ti^{21+} ions to 0.191 for high-Z Au^{78+} ions, i.e., an increase by a factor of 7.64. In addition, it is worth mentioning that for Au^{78+} ions the sign of the anisotropy parameter changes from negative to positive at the impact energy of about 4.2 times the excitation threshold due to the contribution of the Breit interaction, which indicates that a

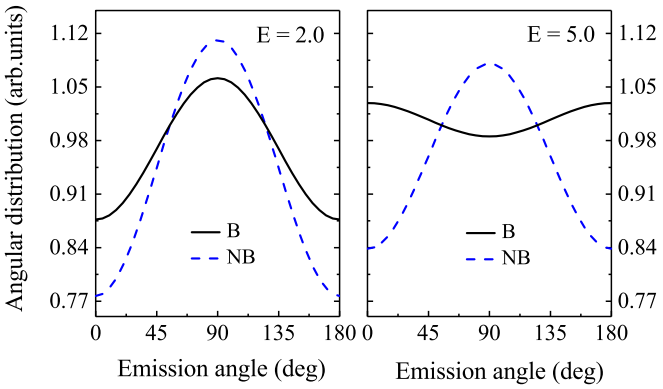

FIG. 6. Angular distribution of the Lyman-α_1 line radiated from Au^{78+} ions for two impact energies, i.e., 2.0 (left) and 5.0 (right) times the excitation threshold 71 764.278 eV. Results are shown for both the NB (blue dashed lines) and B (black solid lines) cases for comparison.

qualitative change occurs in the angular emission pattern of the Lyman-α_1 line, as will be seen below.

To see the angular emission behavior of the Lyman-α_1 line and also to illustrate the effect of the Breit interaction more intuitively, as an example, Fig. 6 shows the angular distribution of the Lyman-α_1 line radiated from Au^{78+} ions for two different impact energies, i.e., 2.0 and 5.0 times the excitation threshold (71 764.278 eV). Once again, results are plotted here for both of the NB and B cases for comparison. As can be clearly seen in Fig. 6, for the NB case the corresponding Lyman-α_1 photons are predominantly radiated under $\theta = 90^\circ$, i.e., perpendicularly to the impact electron beam, even at high impact energies. However, the situation becomes quite different when the Breit interaction is taken into consideration. To be more specific, although the Breit interaction only quantitatively makes the Lyman-α_1 line less anisotropic at low impact energies, a qualitative change occurs in its angular emission pattern at high energies, i.e., from a perpendicularly dominated emission pattern to a forward- and backward-dominated one. Such a qualitative change was obtained also for the angular distribution of characteristic x-ray lines following dielectronic recombination of highly charged lithiumlike ions [2]. On the basis of a deep and detailed analysis of the present results, the obtained forward- and backward-dominated angular emission pattern is expected to be more pronounced at higher impact energies and for higher-Z hydrogenlike ions.

IV. SUMMARY

To summarize, the EIE from the ground state to the excited $2p_{3/2}$ level and the subsequent Lyman-α_1 decay of hydrogenlike Ti^{21+}, Mo^{41+}, Ba^{55+}, and Au^{78+} ions have been studied by using the relativistic distorted-wave method. Special attention has been paid to (the effects of the Breit interaction on) the linear polarization and angular distribution of the Lyman-α_1 line radiated from these ions. To do so, we first calculated the partial EIE cross sections for the excitations to the individual substates $|M_f = \pm 1/2\rangle$ and $|M_f = \pm 3/2\rangle$ of the $2p_{3/2}$ level. The obtained partial EIE cross sections were then utilized to calculate the alignment parameter of the excited $2p_{3/2}$ level and, further, to obtain the linear polarization and angular distribution (i.e., the anisotropy parameter) of the Lyman-α_1 line. It is found that the present partial EIE cross sections and linear polarization agree excellently with the RCCC results [44] available for Ti^{21+} ions, although (more or less) discrepancies with the RDW results of Reed and Chen [39] are obtained for the NB case, especially at low impact electron energies. In the actual case with the Breit interaction considered, the present linear polarization coincides well with the experimental results of Ti^{21+} ions [40] within the experimental uncertainties. In addition, it is found that the Breit interaction makes the substates $|M_f = \pm 1/2\rangle$ less populated, whereas it contributes to populating more the $|M_f = \pm 3/2\rangle$ ones. Moreover, the Lyman-α_1 line is found to be less linearly polarized and less anisotropic due to the contribution of the Breit interaction. Such effects of the Breit interaction on the partial EIE cross sections and on the angular and polarization properties of the Lyman-α_1 line behave more prominently for higher-Z ions and higher impact energies. For instance, the Breit interaction alters even qualitatively the polarization behavior and angular emission pattern of the Lyman-α_1 line radiated from high-Z Au^{78+} ions at the impact energy of about 4.2 times the excitation threshold.

ACKNOWLEDGMENTS

This work has been funded by the National Natural Science Foundation of China under Grants No. 12174315 and No. 11804280, the Chinese Scholarship Council under Grant No. 202008620004, the Youth Science and Technology Talent Promotion Project of Gansu Province under Grant No. GXH2020626-09, the Key Program of the Research Ability Promotion Project for Young Scholars of Northwest Normal University of China under Grant No. NWNU-LKQN2019-5, and the Longyuan Youth Innovation and Entrepreneurship Talent Project of Gansu Province.

[1] N. Nakamura, A. P. Kavanagh, H. Watanabe, H. A. Sakaue, Y. Li, D. Kato, F. J. Currell, and S. Ohtani, Phys. Rev. Lett. **100**, 073203 (2008).

[2] S. Fritzsche, A. Surzhykov, and T. Stöhlker, Phys. Rev. Lett. **103**, 113001 (2009).

[3] Z. W. Wu, J. Jiang, and C. Z. Dong, Phys. Rev. A **84**, 032713 (2011).

[4] Z. Hu, X. Han, Y. Li, D. Kato, X. Tong, and N. Nakamura, Phys. Rev. Lett. **108**, 073002 (2012).

[5] H. Jörg, Z. Hu, H. Bekker, M. A. Blessenohl, D. Hollain, S. Fritzsche, A. Surzhykov, J. R. Crespo López-Urrutia, and S. Tashenov, Phys. Rev. A **91**, 042705 (2015).

[6] C. Shah, H. Jörg, S. Bernitt, S. Dobrodey, R. Steinbrügge, C. Beilmann, P. Amaro, Z. Hu, S. Weber, S. Fritzsche, A. Surzhykov, J. R. CrespoLopez-Urrutia, and S. Tashenov, Phys. Rev. A **92**, 042702 (2015).

[7] N. Nakamura, J. Phys. B: At. Mol. Opt. Phys. **49**, 212001 (2016).

[8] P. Amaro, C. Shah, R. Steinbrügge, C. Beilmann, S. Bernitt, J. R. Crespo López-Urrutia, and S. Tashenov, Phys. Rev. A **95**, 022712 (2017).

[9] Z. W. Wu, M. M. Zhao, C. Ren, C. Z. Dong, and J. Jiang, Phys. Rev. A **101**, 022701 (2020).

[10] A. Gumberidze, D. B. Thorn, A. Surzhykov, C. J. Fontes, D. Bana, H. F. Beyer, W. Chen, R. E. Grisenti, S. Hagmann, R. Hess *et al.*, Atoms **9**, 20 (2021).

[11] J. R. Henderson, P. Beiersdorfer, C. L. Bennett, S. Chantrenne, D. A. Knapp, R. E. Marrs, M. B. Schneider, K. L. Wong, G. A. Doschek, J. F. Seely, C. M. Brown, R. E. LaVilla, J. Dubau, and M. A. Levine, Phys. Rev. Lett. **65**, 705 (1990).

[12] A. Surzhykov, Y. Litvinov, T. Stöhlker, and S. Fritzsche, Phys. Rev. A **87**, 052507 (2013).

[13] Z. W. Wu, A. Surzhykov, and S. Fritzsche, Phys. Rev. A **89**, 022513 (2014).

[14] Z. W. Wu, Z. Q. Tian, J. Jiang, C. Z. Dong, and S. Fritzsche, Phys. Rev. A **102**, 042813 (2020).

[15] S. Tashenov, D. Banaś, H. Beyer, C. Brandau, S. Fritzsche, A. Gumberidze, S. Hagmann, P. M. Hillenbrand, H. Jörg, I. Kojouharov, C. Kozhuharov, M. Lestinsky, Y. A. Litvinov, A. V. Maiorova, H. Schaffner, V. M. Shabaev, U. Spillmann, T. Stohlker, A. Surzhykov, and S. Trotsenko, Phys. Rev. Lett. **113**, 113001 (2014).

[16] M. H. Chen and J. H. Scofield, Phys. Rev. A **52**, 2057 (1995).

[17] S. Tashenov, T. Stöhlker, D. Banaś, K. Beckert, P. Beller, H. F. Beyer, F. Bosch, S. Fritzsche, A. Gumberidze, S. Hagmann, C. Kozhuharov, T. Krings, D. Liesen, F. Nolden, D. Protic, D. Sierpowski, U. Spillmann, M. Steck, and A. Surzhykov, Phys. Rev. Lett. **97**, 223202 (2006).

[18] A. Surzhykov, S. Fritzsche, T. Stöhlker, and S. Tashenov, Phys. Rev. Lett. **94**, 203202 (2005).

[19] S. Tashenov, T. Bäck, R. Barday, B. Cederwall, J. Enders, A. Khaplanov, Y. Poltoratska, K.-U. Schässburger, and A. Surzhykov, Phys. Rev. Lett. **107**, 173201 (2011).

[20] R. Märtin, G. Weber, R. Barday, Y. Fritzsche, U. Spillmann, W. Chen, R. D. DuBois, J. Enders, M. Hegewald, S. Hess, A. Surzhykov, D. B. Thorn, S. Trotsenko, M. Wagner, D. F. A. Winters, V. A. Yerokhin, and T. Stohlker, Phys. Rev. Lett. **108**, 264801 (2012).

[21] A. Surzhykov, S. Fritzsche, A. Gumberidze, and T. Stöhlker, Phys. Rev. Lett. **88**, 153001 (2002).

[22] G. Weber, H. Brauning, A. Surzhykov, C. Brandau, S. Fritzsche, S. Geyer, S. Hagmann, S. Hess, C. Kozhuharov, R. Martin, N. Petridis, R. Reuschl, U. Spillmann, S. Trotsenko, D. F. A. Winters, and T. Stohlker, Phys. Rev. Lett. **105**, 243002 (2010).

[23] Z. W. Wu, N. M. Kabachnik, A. Surzhykov, C. Z. Dong, and S. Fritzsche, Phys. Rev. A **90**, 052515 (2014).

[24] Z. W. Wu, A. V. Volotka, A. Surzhykov, C. Z. Dong, and S. Fritzsche, Phys. Rev. A **93**, 063413 (2016).

[25] Z. W. Wu, A. V. Volotka, A. Surzhykov, and S. Fritzsche, Phys. Rev. A **96**, 012503 (2017).

[26] Z. W. Wu, C. Z. Dong, and J. Jiang, Phys. Rev. A **86**, 022712 (2012).

[27] P. Beiersdorfer, D. A. Vogel, K. J. Reed, V. Decaux, J. H. Scofield, K. Widmann, G. Hölzer, E. Förster, O. Wehrhan, D. W. Savin, and L. Schweikhard, Phys. Rev. A **53**, 3974 (1996).

[28] P. Beiersdorfer, G. Brown, S. Utter, P. Neill, K. J. Reed, A. J. Smith, and R. S. Thoe, Phys. Rev. A **60**, 4156 (1999).

[29] G. K. James, D. Dziczek, J. A. Slevin, and I. Bray, Phys. Rev. A **66**, 042710 (2002).

[30] J. Jiang, C.-Z. Dong, L.-Y. Xie, and J.-G. Wang, Phys. Rev. A **78**, 022709 (2008).

[31] L. Sharma, A. Surzhykov, R. Srivastava, and S. Fritzsche, Phys. Rev. A **83**, 062701 (2011).

[32] C. J. Bostock, D. V. Fursa, and I. Bray, Phys. Rev. A **89**, 062710 (2014).

[33] C. J. Bostock, D. V. Fursa, I. Bray, and K. Bartschat, Phys. Rev. A **90**, 012707 (2014).

[34] C. Ren, Z. W. Wu, J. Jiang, L. Y. Xie, D. H. Zhang, and C. Z. Dong, Phys. Rev. A **98**, 012711 (2018).

[35] Dipti, S. W. Buechele, A. C. Gall, S. Sanders, C. I. Szabo, R. Silwal, E. Takacs, and Y. Ralchenko, J. Phys. B: At., Mol. Opt. Phys. **53**, 115701 (2020).

[36] Z. W. Wu, Z. Q. Tian, Y. H. An, and C. Z. Dong, Astrophys. J. **910**, 142 (2021).

[37] C. Shah, N. Hell, A. Hubbard, M. F. Gu, M. J. MacDonald, M. E. Eckart, R. L. Kelley, C. A. Kilbourne, M. A. Leutenegger, F. S. Porter *et al.*, Astrophys. J. **914**, 34 (2021).

[38] Z. W. Wu, Z. Q. Tian, and C. Z. Dong, Phys. Rev. A **105**, 012815 (2022).

[39] K. J. Reed and M. H. Chen, Phys. Rev. A **48**, 3644 (1993).

[40] N. Nakamura, D. Kato, N. Miura, T. Nakahara, and S. Ohtani, Phys. Rev. A **63**, 024501 (2001).

[41] D. L. Robbins, P. Beiersdorfer, A. Y. Faenov, T. A. Pikuz, D. B. Thorn, H. Chen, K. J. Reed, A. J. Smith, K. R. Boyce, G. V. Brown, R. L. Kelley, C. A. Kilbourne, and F. S. Porter, Phys. Rev. A **74**, 022713 (2006).

[42] P. Beiersdorfer, Phys. Scr. **2009**, 014010 (2009).

[43] C. J. Bostock, D. V. Fursa, and I. Bray, Phys. Rev. A **80**, 052708 (2009).

[44] C. J. Bostock, D. V. Fursa, and I. Bray, Can. J. Phys. **89**, 503 (2011).

[45] J. Jiang, C. Z. Dong, L. Y. Xie, J. G. Wang, J. Yan, and S. Fritzsche, Chin. Phys. Lett. **24**, 691 (2007).

[46] Y. Itikawa, Phys. Rep. **143**, 69 (1986).

[47] H. L. Zhang, D. H. Sampson, and A. K. Mohanty, Phys. Rev. A **40**, 616 (1989).

[48] H. L. Zhang, D. H. Sampson, and R. E. H. Clark, Phys. Rev. A **41**, 198 (1990).

[49] I. P. Grant, *Relativistic Quantum Theory of Atoms and Molecules: Theory and Computation* (Springer-Verlag, New York, 2007).

[50] V. V. Balashov, A. N. Grum-Grzhimailo, and N. M. Kabachnik, *Polarization and Correlation Phenomena in Atomic Collisions* (Kluwer Academic, New York, 2000).

[51] K. Blum, *Density Matrix Theory and Applications*, 3rd ed. (Springer, Berlin/Heidelberg, 2012).

[52] P. Jönsson, X. He, C. Froese Fischer, and I. P. Grant, Comput. Phys. Commun. **177**, 597 (2007).

[53] M. F. Gu, Can. J. Phys. **86**, 675 (2008).

[54] S. Fritzsche, Comput. Phys. Commun. **240**, 1 (2019).

[55] W. R. Johnson and G. Soff, At. Data Nucl. Data Tables **33**, 405 (1985).

[56] T. Shirai, J. Sugar, A. Musgrove, and W. L. Wiese, J. Phys. Chem. Ref. Data, Monograph **8** (1997).